Iranian Journal of Geophysics, 2017, Page 57 - 70

Analysis of updraft velocity in mesoscale convective systems using satellite and WRF model simulations

Reza Khandan[1], Seyed Kazem Alavipanah[2*], Arastoo Pour Biazar[3] and Maryam Gharaylou[4]

[1] *Ph. D. student, Faculty of Geography, University of Tehran, Tehran, Iran*
[2] *Professor, Faculty of Geography, University of Tehran, Tehran, Iran*
[3] *Associate Professor, Atmospheric Science Department, University of Alabama in Huntsville, Huntsville, USA*
[4] *Assistant Professor, Institute of Geophysics, University of Tehran, Tehran, Iran*

(Received: 22 January 2017, Accepted: 24 May 2017)

Abstract

Updraft vertical velocity is an important dynamical quantity which is strongly related to storm intensity and heavy precipitation. It can be calculated by direct observations, NWP model, and geostationary satellites which can provide the possibility of measuring this quantity with high temporal resolution. This research analyzed updraft velocity based on six derived parameters from INSAT3-D and high temporal and spatial resolution simulations of WRF model in the west and southwest of Iran. The interrelationship among the derived variables was investigated from the immature to mature stages of convective cells in Mesoscale Convective Systems (MCS). Updraft velocity was calculated based on a theoretical framework and real observations. The was a large results discrepancy among the results. This finding was in company with previous studies which concluded that updraft velocity is the resultant of other bulk buoyancy forces and environmental variables. Also, the estimated updraft velocities showed a positive correlation with height. The authors proposed linear regression, as a parametric, and Random Forest (RF), as a non-parametric, machine learning methods for estimation of updraft velocity based on satellite variables. A forward–backward method was applied to reach the best modeling in both methods. In linear regression modeling, the cloud-top cooling rate was the most significant factor, and in the RF, band difference of water vapor, thermal infrared 1, and elevation data had the maximum importance. Results showed that the RF could better estimate updraft velocity.

Keywords: MCS, updraft velocity, NWP, geostationary satellite, CAPE

[*]Corresponding author: salavipa@ut.ac.ir

1 Introduction

Convective clouds are one of the major environmental challenges with significant effects on many infrastructures like aviation. Knowledge about microphysics, chemistry, thermodynamics, cloud environment and dynamics of these clouds is of great help for modeling their behaviors. In cloud dynamics, updraft velocity is the main variable which strongly affects the intensity of convective storms. Few field campaigns studied updraft velocities in direct observation by aircraft like the "Midlatitude Continental Convective Clouds Experiment" MC3E (Jensen et al., 2016) and most of the researches were limited to Numerical Weather Prediction (NWP) models and radar observations during the last decades. Xu and Randall (2001) analyzed the updraft and downdrafts of simulated tropical oceanic and midlatitude continental cumulus convections in eastern Atlantic and Oklahoma regions. Parodi and Emanuel (2009) employed WRF model with the assumption of radiative–convective equilibrium in deep moist convection to study updraft velocity. Wang and Zhang (2014) used large-eddy simulation of four shallow convection cases and found that in updraft and cloud plumes, the buoyancy force has the major contribution in the lower and middle parts of clouds, and sub-grid transport is larger in the upper part of cloud; the mean vertical velocity is influenced by buoyancy forcing and sub plume turbulence. Yang et al. (2016) stated that updraft generally increases with height. Tian and Kuang (2016) found that fractional entrainment per unit height in a plume has a negative relationship with vertical velocity. Morrison (2016) studied the relationship between vertical velocity, perturbation pressure, updraft size, and dimensionality for cumulus clouds. Tang et al. (2016) investigated the seasonal and diurnal variability of vertical velocity using NWP models. Schumacher et al. (2015) analyzed vertical velocity of shallow, mid-level and deep convective clouds by radar observations and showed that convective updraft velocities have a positive correlation with cloud height. Giangrande et al. (2016) used radar wind profiler to study updraft velocity, area fraction, and mass flux profiles. They showed that updrafts and downdrafts increase in magnitude with height to mid-levels. They also showed that stronger vertical velocities are significantly related to "convective available potential energy" (CAPE) and lower low–level moisture conditions.

The emergence of satellite remote sensing provides a possibility to survey convective clouds with broader coverage around the world and with different variables. Polar satellites provide suitable spatial and spectral resolution. Geostationary satellites are capable of acquiring data in high temporal resolution. Therefore, it is possible to analyze updraft velocity based on cloud top-cooling rates. In spite of significant advances in studying convective clouds by satellites, few researches have been conducted to study updraft velocity. Luo et al. (2014) used A-Train satellite constellation observations and concluded that in oceanic convection in their data set, smaller updraft velocities were observed and stated that larger vertical velocities tend to carry larger particle cloud droplets to higher altitudes and produce heavier rainfall. Hamada and Takayabu (2016) analyzed the efficiency of linear modeling of 5-minute cloud-top cooling rate and cloud-top height derived from 3-hourly NWP simulations over the ocean south of Japan. Mecikalski et al. (2016) studied the updrafts by GOES super rapid scans. Regarding the different spatio-temporal behavior of clouds in different climate regimes, it is necessary to carry out research in other areas and

determine the relation between the results from satellite and those of NWP models.

In Iran, several studies have analyzed the dynamics of convective systems from the synoptic point of view (Ahmadi-Givi et al., 2006; Mohammadi et al., 2012; Nazaripour et al., 2015). These studies used NWP model outputs, ground stations, and soundings to study the large-scale environmental issues influencing the formation of convective clouds. It is imperative to study the updraft velocity of convective clouds over Iran in different regions to have a better knowledge about the dynamics of convective clouds. The current study used the advantage of high temporal and spatial resolution satellite data and followed three goals: 1) analysis of different band configurations to explain different states of convective clouds, 2) comparison of the proposed theoretical methods in literature for calculation of updraft velocity with real observations, and 3) analysis of two methods to model the updraft velocity based on satellite data.

2 Study area

The analysis in this research was conducted in the west and southwest of Iran (Figure 1). Case studies were selected from 12 to 16 April 2016 when most of the western and southwestern weather stations of Iran had recorded precipitation rates higher than 10 mm per 6 hours. Selected MCSs can be classified as meso-β (20–200 km) type (Figure 2).

3 Data

Satellite data: INSAT3-D is a geostationary satellite located in 84° East over the equator. It contains two sensors for remote sensing studies. Imager has six bands, and sounder has 19 channels. In order to analyze MCSs, two thermal infrared bands (TIR1 and TIR2) and water vapor from Imager were used. Also, Atmospheric Motion Vectors (AMV) known as IRW were used for automatic tracking of convective cells. All data were downloaded via http://www.mosdac.gov.in/ from Meteorological & Oceanographic Satellite Data Archival Centre (MOSDAC).

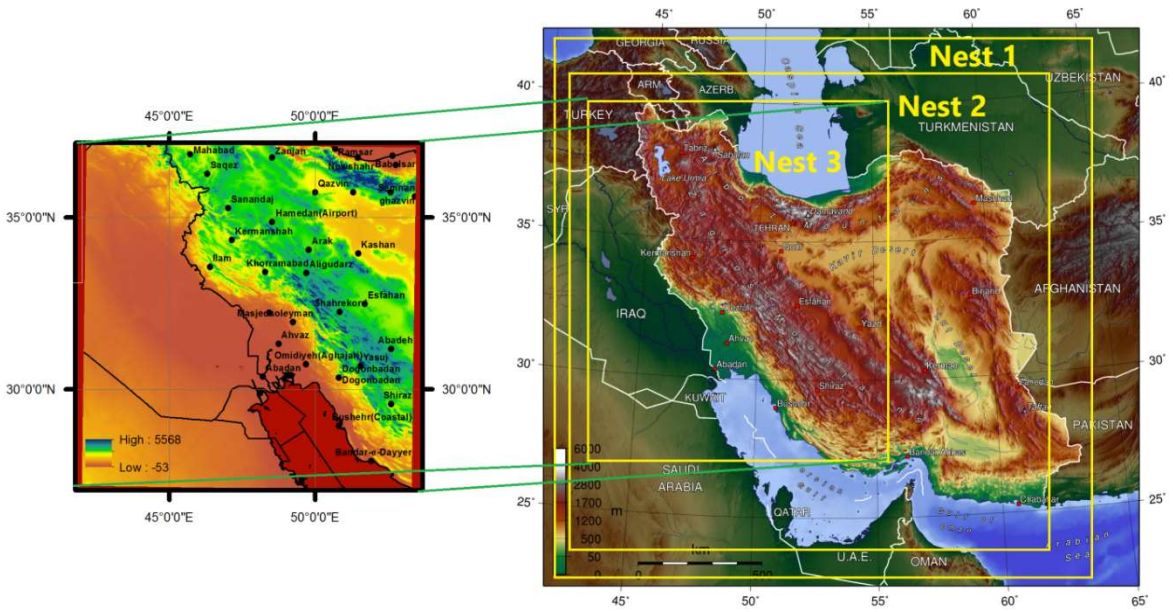

Figure 1. Study area and weather stations in the west and southwest of Iran.

NWP model: The Weather Research and Forecasting (WRF) model is used for simulations. The WRF model is a fully compressible and non-hydrostatic model with a run-time hydrostatic option (Skamarock et al., 2005). The FNL data available every 6h at a spatial resolution of $1^{o}x1^{o}$ have been used to obtain initial and boundary conditions. In order to obtain a high spatial resolution grid of 4 km spacing, three nests were defined and the third nest was configured according to the study area. Since the temporal resolution of the Imager data is 30 min., the WRF model was run with half-hourly history interval from 12 April to 15 April and the first twelve hours were regarded as spin-up. The Kain–Fritsch (Kain, 2004) cumulus parameterization was used in two outer grids and the Thompson scheme (Thompson et al., 2004) was used for modeling microphysics of clouds. The default setting for other physical parametrization schemes was used in the WRF model simulation.

Terrain height: Digital Elevation Model (DEM) data were used from USGS via http://srtm.csi.cgiar.org/SELECTION/inputCoord.asp with 0.5 degree in the study area.

4 Methodology

4.1 Data preparation

In order to analyze the updraft velocity, the following six variables were selected: 1) TIR1 Brightness Temperature (BT), 2) TIR2-TIR1, 3) WV-TIR1, 4) terrain height from DEM, 5) atmospheric temperature profile calculated by the WRF model simulations, and 6) CAPE from WRF model simulations. Based on the weighting functions and spectral response functions of satellite bands, it is possible to measure the cloud top temperature and cooling rate from TIR1 band and cloud thickness from WV-TIR1 and TIR2-TIR1 difference (Ackerman, 1996; Ellrod, 2004; Inoue, 1987; Prata, 1989; Schmetz et al., 1997); In the case of the presence of thin clouds, the TIR1 BT from ground radiation is received. As long as a cloud grows, the amount of radiative BT of cloud top is increased in satellite sensor. WV also indicates BT emitted about 20 to 50 kPa (Soden and Bretherton, 1993); therefore as cloud evolves, their difference tends to zero and in the case of mature cumulonimbus clouds, it takes positive values.

From Imager SGP products, TIR1, WV and TIR2 products were extracted and based on lookup tables provided within products; digital counts were converted to BT. Parallel with these calculations, CAPE and atmospheric temperature profile values were extracted from the WRF model outputs by the NCAR Command Language (NCL) scripts for all grid points and were converted to raster (by inverse distance-weighted (IDW) interpolation method) to provide a continuous search space in the algorithm. Then, all rasters (along with DEM data) were clipped based on the study area to reduce the cost of computation. In the next step, ISO DATA unsupervised classification method was used to identify cloud objects in different growth stages in the TIR1 band. Experimentally, the number of classes in this classification algorithm was determined based on the range of BT in a scene; for BTs ranging from -35 to 0 C°, three classes and for -70 to 0 C°, four classes were selected. The output classes from this stage were used as cloud objects to be tracked from the initial to mature growth stages (before dissipation); it was checked to select those cloud objects which did not experience splitting or merging with other cloud objects (Figure 2).

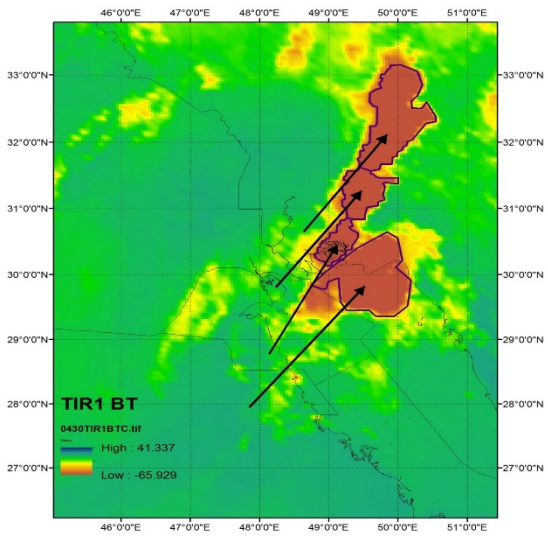

Figure 2. Four sample cloud objects which were tracked to their mature stages (the arrows show their trajectories from their initial growth stages) on 14th April 2016 in the southwest of Iran.

In order to mitigate the effect of neighboring clouds, the mean of quintile of colder pixels in TIR1 and mean of quintile of higher band differences were chosen to be the representative of each cloud object. The mean of terrain height below cloud object was attributed to cloud object. Since CAPE is an environmental variable, a 50 km buffer was used experimentally to search the maximum CAPE around cloud object and use it as its CAPE value; such buffer threshold was calculated based on the displacements between radiosonde measurements and NWP model simulations. In order to calculate the height of cloud by atmospheric temperature profile from the NWP model, the nearest grid point to the coolest pixel in the cloud was chosen.

To automate the tracking process and extract all of the mentioned variables, the method proposed in Walker et al. (2012) was used. AMVs were used to move the objects in the image in the first time (t_1) and make the intersection with objects in the second time (t_2). Those cloud objects in t_2 that had maximum overlap with the moved cloud objects from t_1 were tagged and a history was made for them. Cloud objects were tracked to a time when their top cooling rate ($\Delta\text{TIR1}=\text{TIR1}_{tj}-\text{TIR1}_{ti}$, where tj is $ti+30\,\text{min}$) was positive in the next two consecutive images. All of the mentioned steps were implemented using Python coding and ArcPy library.

4.2 Calculation of updraft velocity

Updraft velocity was calculated based on theory and real data observation. In theory, calculation of updraft velocity was based on pure parcel theory (Dutton, 1976) from the following logic: When a parcel of air passes the level of free convection (LFC), the work W per unit mass done on parcel is expressed as follows:

$$\frac{W}{m}=\int_{LFC}^{z_{\max}}\frac{F}{m}dz=\int_{LFC}^{z_{\max}}a\,dz=-\int_{LFC}^{z_{\max}}g\frac{\Delta\rho}{\rho}dz \\ =\int_{LFC}^{z_{\max}}g\frac{T_{parcel}-T_{env}}{T_{env}}dz\equiv CAPE, \quad (1)$$

where Z_{max} is the altitude where the rising parcel does not have buoyancy and is not warmer than its environment any longer, ρ is the mass density of air parcel and $\Delta\rho$ is the density difference between the parcel and the environment, T_{parcel} is the temperature of the parcel and T_{env} is the temperature of the environment. Considering that when air parcel reaches the LFC, it has velocity gained from the past stages, then the kinetic energy of the parcel becomes:

$$\frac{1}{2}mw^2\left(z_{LFC}\right)+W=\frac{1}{2}mw^2\left(z_{\max}\right). \quad (2)$$

Assuming that the initial velocity at LFC is negligible and from equation (1):

$$\frac{W}{m}=\frac{1}{2}w^2\left(z_{max}\right)=CAPE. \quad (3)$$

Then

$$w(z_{\max}) = \sqrt{2\,CAPE}\,. \quad (4)$$

In order to calculate real updraft velocities, half-hourly cloud top height changes were calculated from the WRF outputs (temperature profiles) and cloud top temperature from TIR1; it was assumed that the emitted cloud top BT was equal to ambient temperature, clouds behaved as black bodies, and atmospheric attenuation effects did not have significant effect on the emitted BT.

In the next step, the retrieved velocities from theory and real observations were compared with each other. To analyze the possibility of modeling vertical velocity based on satellite and the NWP model derived variables, the correlation values between the updraft velocity and TIR1, WV-TIR1, TIR2-TIR1, CAPE, and DEM were analyzed. Then, by considering updraft velocity as a dependent variable, a multivariate regression and the Random Forest (RF) regression methods were used for modeling updraft velocity; RF, first proposed by Ho (1995), is considered as a nonlinear ensemble learning approach which applies multiple weakly correlated decision trees for training. Decision trees are regarded as expert learners. Applying bootstrapping technique makes them powerful in the reduction of high variance which exists in decision trees. In the RF regression, N regression trees are applied by N bootstrapped training sets and the overall average of answers is the final answer. During the process a forward–backward insertion of variables was applied to increase the accuracy of modeling.

The accuracy of modeling was evaluated by cross-validation method; in each modeling method, out of all updraft velocities calculated for all time increments (each updraft velocity calculated from two consecutive satellite observations), one of them was considered for the test and the rest of the updraft velocities were regarded as training data set, then this process was repeated for all of the calculated updraft velocities; the advantage of such cross validation-method is that the training data sets and the test data were changed dynamically and it was possible to include all the calculated updraft velocities both for training and evaluation. Finally, a root mean square error (RSME) was calculated, and the accuracy of both methods was compared, and their significant variables (importance of including variables) were identified.

5 Results

A total number of eighteen convective cells were tracked and their six variables were extracted every half hour. The evolution time of the cells from initial growth to mature stage varied from 2 to 4.5 hours; the total number of satellite observations (time increments) for all eighteen cases was 119. The time series of the data for six variables of the 18 convective cases are shown in Figure 3. Minimum and maximum values of BT in TIR1 were -85.55 C° and 12.63 C° (Figure 3a). The reason for fluctuations in initiation point of tracking was the presence of cirrus clouds which prevents the timely identification of immature cumulus clouds and resulted in a delay in detection of the evolution of convective cloud top temperatures. In fact, clouds were tracked from a point which had negative changes of TIR1. The time series of WV-TIR1 difference are plotted in Figure 3b. The changes vary between -35.56 K and 53.34 K. Also, the changes of TIR2-TIR1 difference were observed between -1.84 K and 20.58 K (Figure 3c). Figure 3e shows the mean terrain height changes below cloud objects, between 0 and 1800m above Mean Sea

Level (MSL). CAPE variability was also between 600.5 and 3074 J/kg (Figure 3e). Most of the time, CAPE showed an almost steady state with no trend, while in mature stages had a decreasing trend. Cloud top height which was calculated from the WRF model and satellite TIR1 BT varied between 2335.9 and 28863 m above MSL (Figure 3f). In order to analyze the interrelationship among variables, their correlations were calculated. Figures 4a, 4d and 4g show that CAPE had low correlations with TIR1, WV-TIR1, and TIR2-TIR1 differences. Base on time series of CAPE (Figure 3e), it can be concluded that CAPE can be regarded simply as an instability index and did not have a linear spatio–temporal relationship with cloud evolution state variables derived from the satellite. DEM had -0.22 correlation with TIR1 (Figure 4b). This is due to the fact that most of the clouds were tracked in the plain lands before reaching

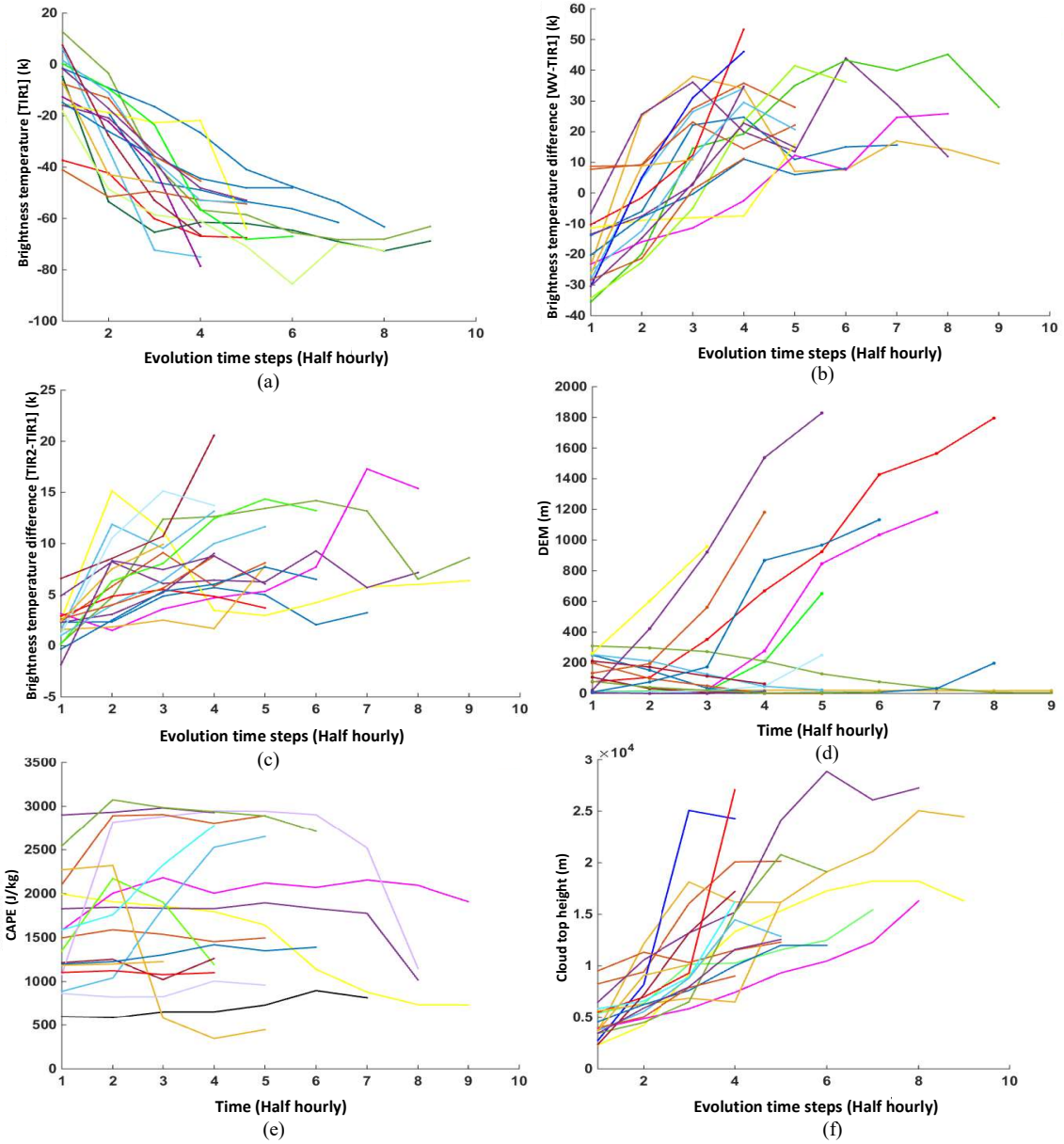

Figure 3. Time series of six variables derived from satellite and the WRF model simulations for 18 cloud objects and 119 observations.

mountainous regions in the west and southwest of Iran. But from the pattern of scatter plots it can be concluded that DEM had a negative effect on TIR1 BT. Among satellite derived cloud evolution variables, TIR1, TIR2-TIR1, and WV-TIR1 had the highest correlations (Figure 4c). Although these variables showed high correlation and it is possible to choose one of them as an indicator of cloud state, it should be kept in mind that WV-TIR1 and TIR2-TIR1 are proxies for removing cirrus clouds and are indicators of cloud thickness.

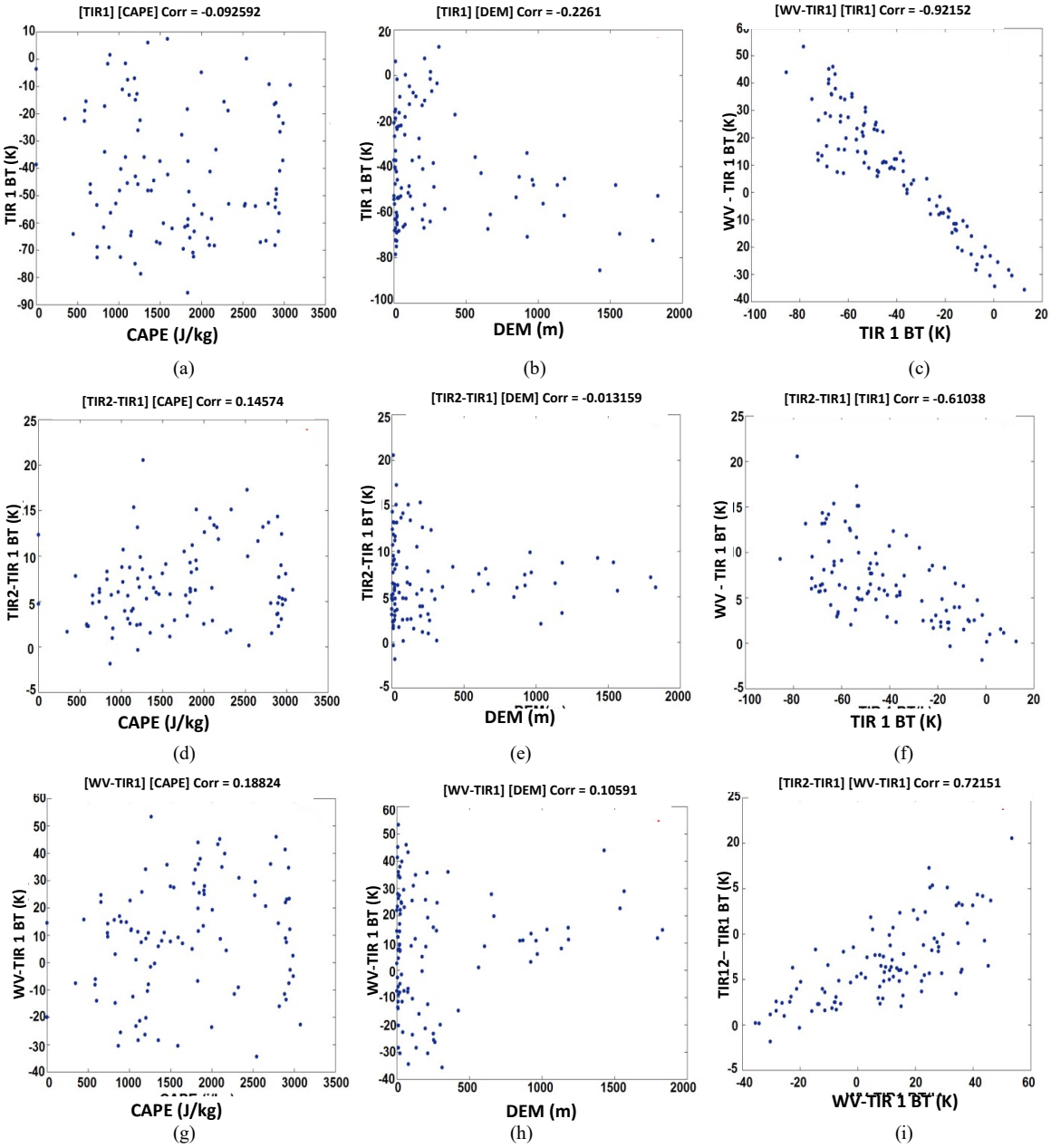

Figure 4. Correlation among the six variables derived from satellite and the WRF model simulations.

5.1 Comparison of updraft velocities calculated by theory and real observations

According to Equation (2), the velocity at Z_{max} is the sum of initial updraft velocity and the work done on a parcel from LFC to Z_{max}. Therefore, it can be regarded as the maximum speed of the parcel. In order to calculate the maximum updraft velocity by theory, at first the time increment with maximum velocity in real time series were found ($t_{\max}$). Then, the values of CAPE in times before and after that time increment ($t_{\max}-30, t_{\max}, t_{\max}+30$ min) were averaged and the maximum values of updraft velocity were calculated based on equation (4) and were compared with the maximum velocity in real observed time series data. The histogram of real velocity observations is shown in Figure 5a. The real vertical velocity varied between 0 to 10 $\mathrm{m\,s^{-1}}$. Negative values can be attributed to dissipation of one cell and growth of another cell in sub pixel resolution which happened within time increments. As Figure 5b shows, the differences between the theoretical and real updraft calculations were large and no strong relationship was observed between the two obtained vertical velocities in each convective case. It can be concluded that in our data set, CAPE was not the only driving force of buoyancy and other factors affected the parcel updraft velocity.

5.2 Updraft velocity estimation

Modeling the updraft velocity based on satellite and NWP derived parameters demands analyzing their relation to updraft velocity. Scatter plots and correlations of changes of each parameter in time increments with updraft velocity are shown in Figure 6. Maximum correlation is observed for TIR1 BT (-0.78) (Figure 6a). This shows that there is a significant linear relationship between updraft velocity and TIR1 BT. In order of significance, the next relationships are for WV-TIR1 (0.62), TIR2-TIR1 (0.38), DEM (0.33), and CAPE (0.08), respectively (Figures 6b, 6c, 6d, and 6e). CAPE scatter plot shows a constant linear behavior along with horizontal axis. This shows that CAPE did not have significant changes in comparison with updraft velocity changes. Figure 6f shows the trend of vertical velocity with altitude; it demonstrates that they have a positive correlation and vertical velocity was increased by increasing altitude.

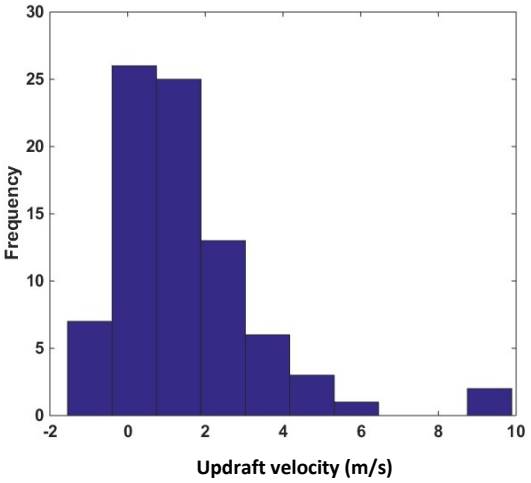

(a)

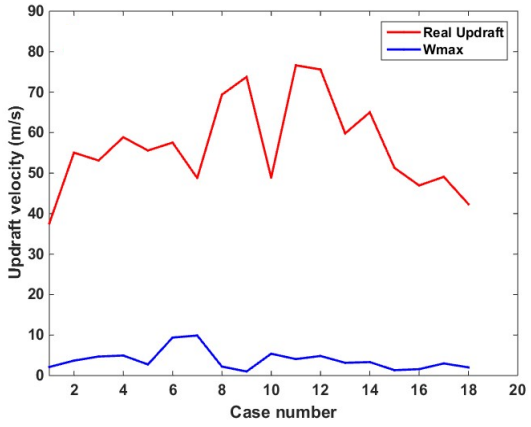

(b)

Figure 5. (a) Histogram of maximum real vertical velocities in whole tracking time of 18 cloud objects and (b) comparison of real and theoretically-derived maximum updraft velocities in the whole tracking time of 18 cloud objects.

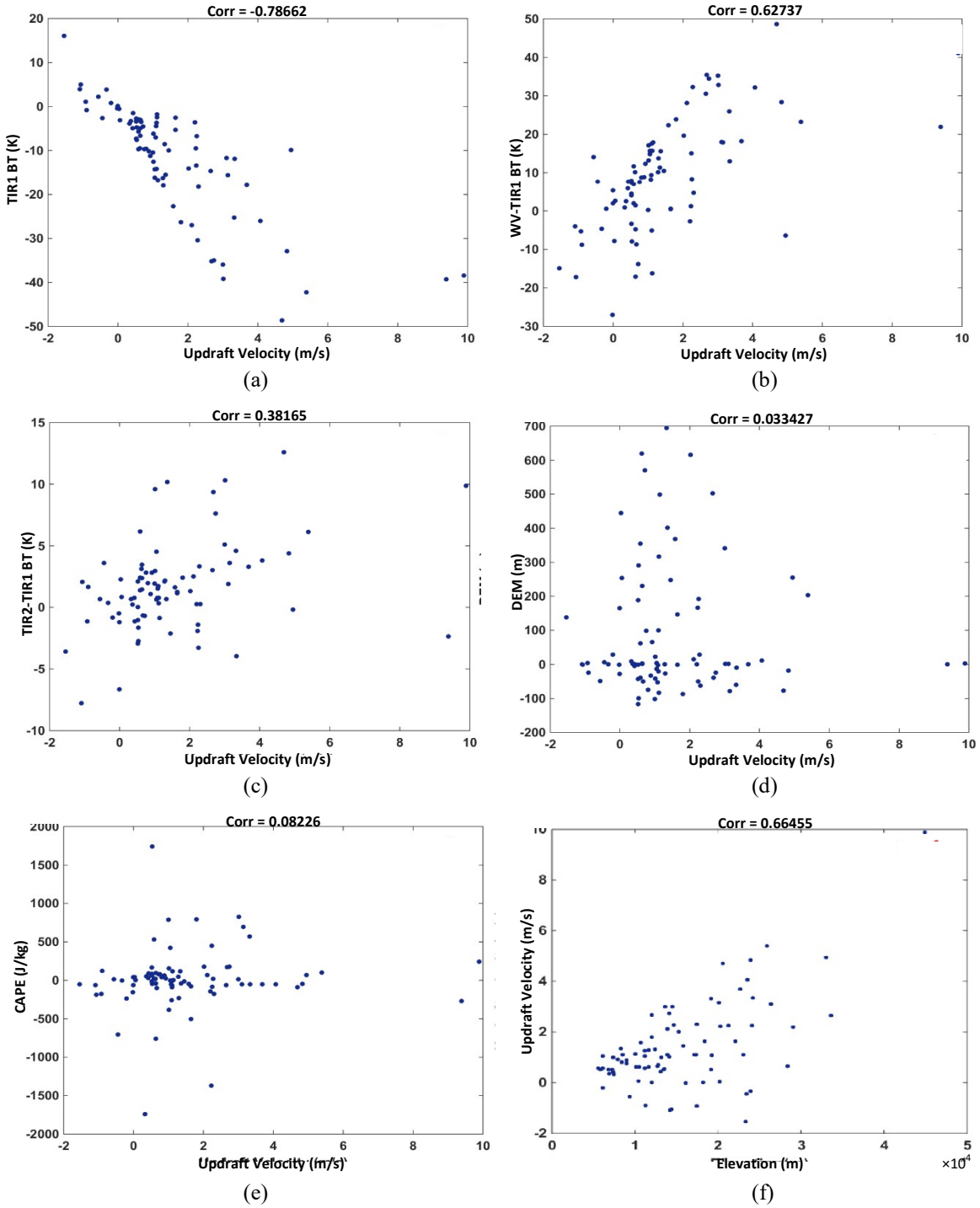

Figure 6. Scatter plots and correlations of updraft velocity with other variables.

In the next step, multivariate linear regression model and RF results were applied to explore the linear and nonlinear effects of parameters and their importance in updraft velocity prediction by forward–backward insertion. Implementation of forward–backward insertion in multi-linear regression showed that only BT cooling rate in TIR1 can estimate vertical velocity with low error. Minimum calculated RMSE in cross-validation procedure for this variable was 1.32 ms^{-1} (Figure 7b). Equation (5) shows the linear regression

model fitted to TIR1 BT time trend between two consecutive times:

$$w = 0.0581 - 0.148\,\Delta TIR1_{j,i}. \quad (5)$$

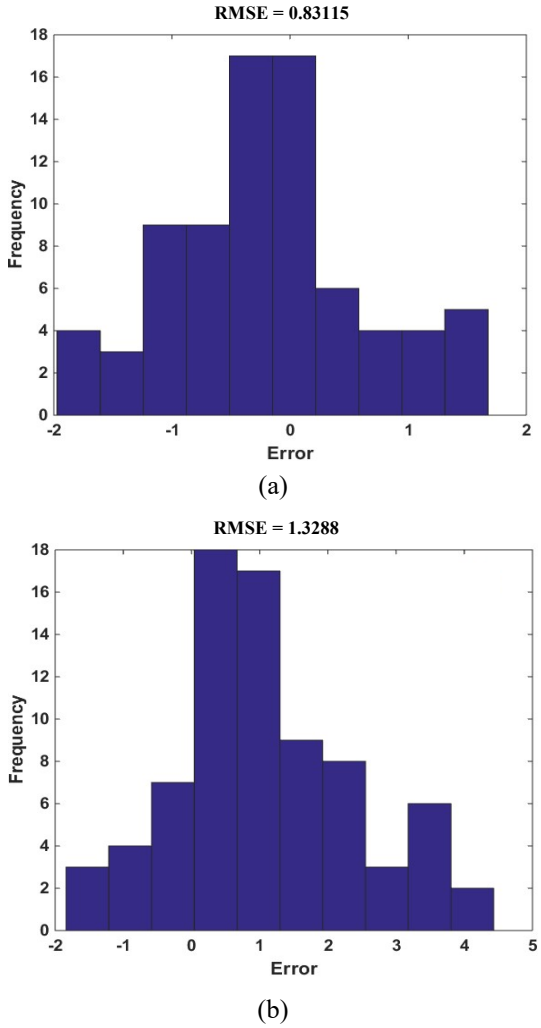

Figure 7. (a) RMSE histogram of the RF in cross validation, (b) RMSE histogram of linear regression in cross validation.

To run the RF, number of trees and predictors in trees should be considered. Determination of the number of trees is based on the volume of data set and improvement of results happen in a specific range. If the number of trees is lower and upper than a specific range, then performance becomes degraded (McGovern et al., 2011). Defining a suitable number of predictors is also important. If all predictors in a tree are selected, then the decision tree method is called Bootstrap Aggregation or Bagging. In RF, the number of predictors is decreased to reduce the correlation among the decision trees. The number of trees was chosen between 5 and 50. The results showed that based on the data set, number of trees between 10 and 20 could provide more accurate results. The number of predictors was chosen as the square of the total number of predictors based on James et al. (2013). Application of the forward–backward procedure in the RF method showed WV-TIR1, TIR1and DEM had the highest importance, respectively. Removal of one of these parameters or adding TIR2-TIR1 increases the RMSE. The RF results performed better in cross-validation procedure. The RMSE of the RF cross validation was 0.83 $\mathrm{m\,s^{-1}}$ (Figure 7a). This shows that since the variables had a dynamic variability in different conditions, a nonlinear machine learning method could provide better results.

6 Discussion

To analyze vertical velocity in convective cells in MCSs, six variables were defined: 1) TIR1 BT, 2) TIR2-TIR1, 3) WV-TIR1, 4) terrain height from DEM, 5) atmospheric temperature profile, and 6) CAPE. Analysis of TIR1 BT time series showed that cloud evolution from immature to mature did not have a constant cooling rate and in some cases a delay may happen. Therefore, clouds were tracked from a point which had a constant cooling rate. Cirrus clouds are also major limitations in detection of immature cells. For these two reasons, the cloud tracking time series range is reduced. Correlation among the six variables showed high values for TIR1, WV-TIR1 and TIR2-TIR1. It was outlined that although they had high correlations, WV-TIR1 and TIR2-TIR1 have the ability to be used as a proxy for

cirrus cloud masking in cloud classification step. Time series plots and correlations of CAPE showed no linear relationship with three satellite derived variables. Based on the data set, it can be stated that CAPE can be regarded only as a bulk buoyancy forcing which its changes are not necessarily involved in direct and abrupt changes of satellite derived variables. Since most cases were tracked in flat lands, it was very hard to suggest any conclusion about the contribution weight of terrain hight on updraft velocity but it may be stated that it is an effectvie element in cloud cooling rate due to orographic forcing. The scatter plot of updraft velocity with altitude showed that updraft velocity increased in higher altitudes. This fact was in company with previous studies (Giangrande et al., 2016; Parodi and Emanuel, 2009; Wang and Zhang, 2014; Xu and Randall, 2001). Comparison of updraft velocities from the theoretical framework and real observations showed large discrepancies. The estimated velocities based on CAPE were between 38 and 77 ms^{-1} wherease real observation velocities were between 0 and 10 ms^{-1} This was in line with recent studies confirming that along with CAPE, other bulk parameters such as deep tropospheric wind shear and environmental variables such as vertical distribution of buoyancy, mixed layer and moist layer depths, environmental temperature, temperature at the cloud base, height of LFC, vertical distribution of buoyancy, and terminal velocity of raindrops affect updraft velocity (Adlerman and Droegemeier, 2005; Cohen and McCaul Jr, 2006; Kirkpatrick et al., 2009; McCaul Jr and Cohen, 2002; McCaul Jr et al., 2005; McCaul Jr and Weisman, 1996; Parodi and Emanuel, 2009; Weisman and Klemp, 1982, 1984). Therefore, it can be stated that vertical velocity is resultant of many parameters but since it is manifested as cooling rate in satellite images, it is possible to measure it by satellite derived signatures. A multilinear regression was fitted and a forward–backward variable insertion was applied. The RMSEs derived from cross validation showed that only TIR1 BT could represent lower RMSE results. The RF, as a nonlinear machine learning method, was employed and the results showed better accuracy. This suggests the nonlinear relationship among variables should be considered. Based on the RF results, the important variables for updraft velocity estimation were identified as WV-TIR1, TIR1, and DEM, respectively.

7 Conclusions

Updraft vertical velocity of convective cells was estimated by employing high spatial and temporal resolution NWP model outputs and INSAT3-D data and the theoretical framework presented in the literature. The results showed that the theoretical framework for estimation of updraft velocity had large errors and along with CAPE other bulk buoyancy forcings and environmental parameters affect vertical velocity. The estimated range of updraft velocities for the applied data set was between 0 to 10 $m\,s^{-1}$ which was positively correlated with height. This research proposed two methods for fast updraft velocity estimation to study MCSs: 1) linear regression by cloud cooling rate; 2) RF by WV-TIR1, TIR1, and DEM. The results also showed that the linear relationship had lower estimation accuracy and the nonlinear machine learning algorithms can better estimate the output. By applying more case studies in future in other parts of Iran, it is possible to provide more training sets and improve the accuracy of updraft velocity estimation. Also, The recent repositioning of Meteosat-8 over Indian Ocean provides a higher spectral and temporal resolution for studying

convective cloud dynamics. A comprehensive research is needed in future to analyze and calibrate satellite cloud products like cloud top pressure and cloud base height with NWP model and ground observations to study the dynamics of convective cells with different updraft mechanisms.

Acknowledgment

The authors are thankful to Oceanographic Satellite Data Archival Centre (MOSDAC) for providing access to the L1C-SGP and L2P-IRW products. Dr. Omid Alizadeh and Dr. Majid Azadi are deeply acknowledged for providing access to input data, software and hardware facilities for running WRF NWP model.

References

Ackerman, SA., 1996, Global Satellite Observations of Negative Brightness Temperature Differences between 11 and 6.7 μm: Journal of the Atmospheric Sciences, **53**(19), 2803-2812.

Adlerman, EJ., & Droegemeier, KK., 2005, The Dependence of Numerically Simulated Cyclic Mesocyclogenesis Upon Environmental Vertical Wind Shear: Monthly Weather Review, **133**(12), 3595-3623.

Ahmadi Givi, F., Mohebalhojeh, AR., & Gharaylou, M., 2006, The Dynamics of Cyclonic Systems over Iran Using Potential Vorticity Diagnostics; A Case Study for Nov-Dec 2003: Earth and Space Physics, **32**(1), 13.

Cohen, C, & McCaul Jr, EW.2006. The Sensitivity of Simulated Convective Storms to Variations in Prescribed Single-Moment Microphysics Parameters That Describe Particle Distributions, Sizes, and Numbers. Monthly Weather Review, **134**(9), 2547-2565.

Ellrod, GP.2004. Impact on Volcanic Ash Detection Caused by the Loss of the 12.0 Mm "Split Window" Band on Goes Imagers. Journal of volcanology and geothermal research, **135**(1), 91-103.

Giangrande, SE, Toto, T, Jensen, MP, Bartholomew, MJ, Feng, Z, Protat, A, . . . Machado, L.2016. Convective Cloud Vertical Velocity and Mass-Flux Characteristics from Radar Wind Profiler Observations During Goamazon2014/5. Journal of Geophysical Research: Atmospheres, **121**(21).

Hamada, A, & Takayabu, YN.2016. Convective Cloud Top Vertical Velocity Estimated from Geostationary Satellite Rapid-Scan Measurements. Geophysical Research Letters, **43**(10), 5435-5441.

Inoue, T.1987. An Instantaneous Delineation of Convective Rainfall Areas Using Split Window Data of Noah-7 Avhrr. Journal of the Meteorological Society of Japan. Ser. II, **65**(3), 469-481.

James, G, Witten, D, Hastie, T, & Tibshirani, R. 2013. An Introduction to Statistical Learning (Vol. 6): Springer.

Jensen, MP, Petersen, WA, Bansemer, A, Bharadwaj, N, Carey, L, Cecil, D, Gerlach, J.2016. The Midlatitude Continental Convective Clouds Experiment (Mc3e). Bulletin of the American Meteorological Society, **97**(9), 1667-1686.

Kain, JS.2004. The Kain–Fritsch Convective Parameterization: An Update. Journal of Applied Meteorology, **43**(1), 170-181.

Kirkpatrick, C, McCaul Jr, EW, & Cohen, C.2009. Variability of Updraft and Downdraft Characteristics in a Large Parameter Space Study of Convective Storms. Monthly Weather Review, **137**(5), 1550-1561.

Luo, ZJ, Jeyaratnam, J, Iwasaki, S, Takahashi, H, & Anderson, R.2014. Convective Vertical Velocity and Cloud Internal Vertical Structure: An a-Train Perspective. Geophysical Research Letters, **41**(2), 723-729.

McCaul Jr, EW, & Cohen, C.2002. The Impact on Simulated Storm Structure and Intensity of Variations in the Mixed Layer and Moist Layer Depths. Monthly Weather Review, **130**(7), 1722-1748.

McCaul Jr, EW, Cohen, C, & Kirkpatrick, C.2005. The Sensitivity of Simulated Storm Structure, Intensity, and Precipitation Efficiency to Environmental Temperature. Monthly Weather Review, **133**(10), 3015-3037.

McCaul Jr, EW, & Weisman, ML.1996. Simulations of Shallow Supercell Storms in Landfalling Hurricane Environments. Monthly Weather Review, **124**(3), 408-429.

Mecikalski, JR, Jewett, CP, Apke, JM, & Carey, LD.2016. Analysis of Cumulus Cloud Updrafts as Observed with 1-Min Resolution Super Rapid Scan Goes Imagery. Monthly Weather Review, **144**(2), 811-830.

Mohammadi, H, Fattahi, E, Shamsi pour, AA, & Akbari, M.2012. Dynamic Analysis of Sudan Low-Pressure Systems and Torrents in Southwest of Iran.

Morrison, H.2016. Impacts of Updraft Size and Dimensionality on the Perturbation Pressure and Vertical Velocity in Cumulus Convection.

Part Ii: Comparison of Theoretical and Numerical Solutions and Fully Dynamical Simulations. Journal of the Atmospheric Sciences, **73**(4), 1455-1480.

Nazaripour, H, Dostkamiyan, M, & Alizadeh, S.2015. The Spatial Distribution Patterns of Temperature, Precipitation, and Humidity Using Geostatistical Exploratory Analysis (Case Study: Central Area of Iran).

Parodi, A, & Emanuel, K.2009. A Theory for Buoyancy and Velocity Scales in Deep Moist Convection. Journal of the Atmospheric Sciences, **66**(11), 3449-3463.

Prata, A.1989. Observations of Volcanic Ash Clouds in the 10-12 Mm Window Using Avhrr/2 Data. International Journal of Remote Sensing, **10**(4-5), 751-761.

Schmetz, J, Tjemkes, S, Gube, M, & Van de Berg, L.1997. Monitoring Deep Convection and Convective Overshooting with Meteosat. Advances in Space Research, **19**(3), 433-441.

Schumacher, C, Stevenson, SN, & Williams, CR.2015. Vertical Motions of the Tropical Convective Cloud Spectrum over Darwin, Australia. Quarterly Journal of the Royal Meteorological Society, **141**(691), 2277-2288.

Skamarock, WC, Klemp, JB, Dudhia, J, Gill, DO, Barker, DM, Wang, W, & Powers, JG. (2005). A Description of the Advanced Research Wrf Version 2. Retrieved from

Soden, BJ, & Bretherton, FP.1993. Upper Tropospheric Relative Humidity from the Goes 6.7 Mm Channel: Method and Climatology for July 1987. Journal of Geophysical Research: Atmospheres, **98**(D9), 16669-16688.

Tang, S, Xie, S, Zhang, Y, Zhang, M, Schumacher, C, Upton, H, . . . Ahlgrimm, M.2016. Large-Scale Vertical Velocity, Diabatic Heating and Drying Profiles Associated with Seasonal and Diurnal Variations of Convective Systems Observed in the Goamazon2014/5 Experiment. Atmospheric Chemistry and Physics, **16**(22), 14249.

Thompson, G, Rasmussen, RM, & Manning, K.2004. Explicit Forecasts of Winter Precipitation Using an Improved Bulk Microphysics Scheme. Part I: Description and Sensitivity Analysis. Monthly Weather Review, **132**(2), 519-542.

Tian, Y, & Kuang, Z.2016. Dependence of Entrainment in Shallow Cumulus Convection on Vertical Velocity and Distance to Cloud Edge. Geophysical Research Letters, **43**(8), 4056-4065.

Walker, JR, MacKenzie Jr, WM, Mecikalski, JR, & Jewett, CP.2012. An Enhanced Geostationary Satellite–Based Convective Initiation Algorithm for 0–2-H Nowcasting with Object Tracking. Journal of Applied Meteorology and Climatology, **51**(11), 1931-1949.

Wang, X, & Zhang, M.2014. Vertical Velocity in Shallow Convection for Different Plume Types. Journal of Advances in Modeling Earth Systems, **6**(2), 478-489.

Weisman, ML, & Klemp, JB.1982. The Dependence of Numerically Simulated Convective Storms on Vertical Wind Shear and Buoyancy. Monthly Weather Review, **110**(6), 504-520.

Weisman, ML, & Klemp, JB.1984. The Structure and Classification of Numerically Simulated Convective Stormsin Directionally Varying Wind Shears. Monthly Weather Review, **112**(12), 2479-2498.

Xu, K-M, & Randall, DA.2001. Updraft and Downdraft Statistics of Simulated Tropical and Midlatitude Cumulus Convection. Journal of the Atmospheric Sciences, **58**(13), 1630-1649.

Yang, J, Wang, Z, Heymsfield, AJ, & French, JR.2016. Characteristics of Vertical Air Motion in Isolated Convective Clouds. Atmospheric Chemistry and Physics, **16**(15), 10159-10173.